Header will be provided by the publisher

Free-standing Nanoparticle Superlattice Sheets: From Design to Applications

WENLONG CHENG[1,2]

[1] *Department of Chemical Engineering, Faculty of Engineering, Monash University, Clayton 3800, Victoria, Australia*
[2] *The Melbourne Centre for Nanofabrication, 151 Wellington Road, Clayton 3168, Victoria, Australia*

received and accepted dates provided by the publisher
other relevant dates provided by the publisher

PACS 81.16.Dn – First pacs description
PACS 68.65.Cd – Second pacs description
PACS 81.07.Bc – Third pacs description

Abstract – Here I summarize my perspective in free-standing nanoparticle superlattice sheets with regards to their fabrication, properties, and applications.

Why free-standing? – Nanoparticles have been coined as "artificial atoms" due to their unique size/shape-dependent optical, electrical, magnetic and conductive properties. Encouraging progress made over the past several decades allows for controlling nanoparticles sizes and shapes, enabling the formation of so-called "artificial periodic table".1 Crystallization of these artificial atoms into highly-ordered arrays represents a unique strategy to design metamaterials with collective properties different from those of bulk phase crystals, isolated nanocrystals and even disordered nanocrystal assemblies.2-6 These unusual properties include spin properties,7 metal-insulator transition,2 mechanical properties,4, 8 p-type conductivities,5 vibrational coherence, 3 and plasmonic properties.9-11 In addition, diverse types of lattice structures have been found including face-centered cubic, body-centered cubic, hexagonal-closed packed, diamond-like lattice, and lattice structures not existing in nature.12

It has to be noted that majority of these studies focus on solid substrate-supported nanoparticle superlattices or solution-state nanoparticle superlttices. In contrast, free-standing nanoparticle superlattice sheets refer to suspended ordered nanoparticle arrays with minimal contact with solid substrate. Compared to dominant solid substrate-supported or solution-state systems, free-standing nanoparticle superlattice sheets offers the advantages of facile transferring, manufacturable into 1D or 3D structures, and application as ion-permeable membranes.

Transferrable. In comparison to their counterparts in substrate-supported or solution-state system, free-standing nanoparticle superlattices offer the unique advantage of facile transfer from one substrate to another. Fig.1 shows the transfer of Langmuir-deposited gold nanowire superlattice membranes from air/water interface from PDMS substrate to PET substrate. One can see that monolayered nanowire membranes can be transferred onto PET substrate with 100% transfer fidelity.13 This facile transfer was also demonstrated to be feasible for transferring plasmene nanosheets onto paper-based Maylasian banknote, Australian plastic banknote, and even rigid topologically complex rigid surfaces such as coins. 14, 15 It is even possible to obtain free-standing bilayered nanoparticle superlattice sheets.16

Manufacturable into 1D and 3D structures. Another unique attribute of free-standing system is that they can be further manufactured into complex structurally well-defined one-dimensional and three-dimensional nanoarchitectures, which is often challenging to obtain from substrate-supported or solution-state system. As an example, suspended polystyrene-based nanoparticle superlattices can be transformed into 1D nanoribbons simply using 'hard milling' by focused ion beam (FIB) lithography. The hard milling means that both organic ligand and inorganic core materials are removed. On the other hand, soft milling involves the use of FIB in a mild condition (either weak beam currents and/or short dwelling time), which can be controlled to remove soft ligand materials only. Combination of hard and soft FIB milling at the programmed locations allows for versatile nanomanufacture of 3D orgami.9, 17 Fig. 1D shows the sequential soft milling applied to polystyrene-based nanoparticle superlattice sheets. Note that site-specific soft ligand removal by soft FIB milling generates local stress. Along the stress relaxation, the nanosheets can self-fold into well-defined origami (Fig. 1d), which has not yet been realized with entirely inorganic 2D materials.

Ion permeable membranes. Free-standing nanosheets also offer the attribute of ion permeability and/or regulation. Using bilayered nanoparticle superlattice sheets, one can fabricate an artificial membrane based on an asymmetric structure, which

(a)E-mail: xyxyxyxyx@xyxy.com
(b)Present address: Author's Instute, Author's University - Street and number, Postal Code City, Country.

can direct unidirectional ionic transport similar to natural cell membrane.16 The asymmetric geometry can be controlled by using two different particle sizes, which leads to the cone-like nanochannels formed within the membranesm (Fig. 2). This results in an asymmetric ion transport behavior, and diode-like behavior. Ionic rectification ratios can be controlled by adjusting relative particle sizes. The free-standing particle sheet-based design of nanomembrane may lead to promising plications biosensor devices, energy conversion, biophotonics, and bioelectronics.

How to fabricate free-standing nanoparticle superlattice sheet? – The formation of free-standing nanoparticle superlattice sheets requires a balance between attraction force and repulsion forces among nanoparticles, which can be achieved either via entropy-driven strategy or enthalpy-driven approach.

Entropy-driven strategy. Drying-mediated self-assembly has demonstrated to be a powerful and general strategy to fabricate ordered assemblies of nanoparticles.2-5 To achieve ordered structures, nanoparticles need to be highly repulsive. Slow evaporation of solvents is usually required to gradually restrict the available volume for each individual nanoparticles to control ordered nucleation and growth process. However, one-dimensionally confined physical environments are required for two-dimensional nucleation and growth in order to obtained two-dimensional free-standing nanoparticle superlattice sheets.4, 8 Alkyl-capped gold nanoparticles and polystyrene-capped plasmonic nanoparticles are hydrophobic, which have been successfully used to generate giant nanosheets (i.e. nanoscale thickness yet with macroscopic lateral dimensions, corresponding to large aspect ratio) from a two-stage drying process (Fig. 3a).4, 9 In the first-stage drying, organic solvents quickly evaporate leaving nanoparticle patches formed at the air/water interface; in the second stage drying, water slowly evaporates offering strong surface tension causing coalesce and fusion of small patches of nanoparticle superlattice sheets into giant ones.

Interestingly, hydrophilic nanoparticles can also be used to generate free-standing nanoparticle superlattice sheets, however, strategies need to be devised to confine crystallization events to a two-dimensional plane. DNA-capped gold nanoparticles have been successfully used to generate nanosheets through microhole-confined self-assembly.8 When a droplet of DNA-nanoparticle solution dries on a holey substrate, satellite microdroplets are formed and trapped in individual microholes owing to pinning of their contact lines onto the microhole edges. Then the microhole-trapped satellite microdroplets thinnes as water evaporates, forming a two dimensional water film which confines crystallization of nanoparticles. Finally, ordered nanoparticle superlattice sheets are suspended in the microholes. This approach allows for simultaneous internal structural control such as interparticle spacing.

Enthalpy-driven strategy. Free-standing nanosheets can also be constructed via enthalpy-driven self-assembly. DNA has been successfully used to program synthesis of free-standing nanosheets. In one example, a DNA sequence with spacing region and self-palindramic region is used to conjugate to gold nanoparticle surfaces.18 Usually, such kind of DNA-capped nanoparticles won't self-assemble into two-dimensional nanosheets in bulk solution. However, it is found that they can form at the air/water interface of a sessile droplet at the optimum ionic strength (Fig. 3b). We have used Synchrotron beam parallel to substrate to raster scan the sessile droplet and record small-angle X-ray scattering (SAXS) patterns. Unlike grazing-incidence SAXS, this parallel SAXS allows for spatial mapping of crystallization events across the entire droplet. Our results reveal the formation of Gibbs monolayer of nanoparticle superlattice sheets. The crystalline sheets at air/water interface can be regulated by adjusting both ionic strength and DNA sequence length. The interparticle spacing changes can be predicted by a modified form of the Daoud–Cotton model. In another example, the programmable DNA-directed self-assembly is combined with the layer-by-layer (LbL) thin film fabrication technique.19 This approach allows for the formation of multidomained films specific to particular surrounding temperature (Fig. 3c). The domain in contact with supporting substrate can be sacrificial by setting appropriate temperature so that the rest of domains remain undisolved, hence, large area free-standing films of DNA-modified gold particles can be obtained. Furthermore, this approach can be combined with top-down lithography to obtain a shape changing film.20 Films can be designed to consist of an active and a passive layer, which can show reversible curling in response to stimulus DNA strands added to solution. With two independently addressable active layers, it is possible to achieve repeatable transformations, involving eight mechanochemical states.

Characterization. – Morphological studies. Nanoparticle superlattice sheets may be characterized by multiscale scales. Naked eye can identify the colors of various plasmonic films with better resolution from optical microscopy.9, 15, 21, 22 To visualize individual particle building blocks and overall structures, transmission electron microscope (TEM) is usually required (Fig. 4a and b). By tilting substrates and recording a serious of two-dimensional TEM images, a 3D tomographic TEM image may be obtained (Fig. 4c, d). Morphological characterization can also be done with atomic force microscopy (AFM). Fig, 4e-g show that both intact and ruptured nanosheets can be identified and high-resolution AFM image shows the ordered nanoparticle arrays (Fig. 4f).

Crystalline structures. Unlike conventional X-ray techniques, high flux of X-ray from Synchrotron can enable acquisition of crystalline information almost instantaneously. Hence, Synchrotron-based SAXS has demonstrated to be a powerful tool to probe in real-time temporal and spatial crystallization events.18, 23 While transmission SAXS have been used to probe crystallization events in bulk solutions,24 grazing-incidence SAXS can be used to monitor the formation of 2D nanoparticle superlattices.18 As an example, using grazing-

incidence SAXS in a special configuration (parallel SAXS, or parSAXS), we can map the crystallization of DNA-capped nanoparticles by raster scanning across a sessile droplet. This can be done in a humidity-controlled environment (Fig. 5). The results reveal the formation of crystalline Gibbs monolayers of DNA-capped nanoparticles at the air–liquid interface. By integrating original two-dimensional SAXS patterns, one can obtain one-dimensional pattern with well-defined Bragg peaks, which then allow for analysis of crystalline lattice structures and other key parameters such as nearest neighbor spacing.

Properties. – *Plasmonic properties*. Due to size- and shape-dependent plasmonic properties, noble metal nanoparticles can be treated as "meta-atoms". When those meta-atoms are closely-packed in the extended 2D arrays, both gap-mode plasmons and propagating plasmons are present.9 Fig. 6a shows a typical TEM image of Au@Ag nanocube plasmene nanosheet, which was imported into COMSOL for exact plasmonic modelling. The modelling result is shown in Fig.6b, where a strong gap-mode plasmon hot spot is evident. This gap-mode plasmons may be responsible for the sharp plasmonic peak observed (Fig. 6c). This peak gets sharper as silver coating thickness increases, which is in agreement with the COMSOL modelling results. On the top of plasmene nanosheet, propagating plasmons are also present as demonstrated theoretically and experimentally. It turns out that plasmene nanosheets support only transverse electric field, leading to the conversion of unpolarized light into polarized light.

Mechanical properties. Unlike traditional colloidal crystals, free-standing ligand-linked nanoparticle superlattice sheets are elastic.4, 8 They can serve as drumhead or mechanical resonators.25 The change of soft ligand length enables the tuning of mechanicl properties. As the ultrathin two-dimensional materials, key micromechanical parameters such as the elastic modulus, ultimate strength, and maximum elongation, can be in principle derived from mechanical tests, such as bulge tests, analysis of buckling deformations, force spectroscopy, and stretching ridge analysis.26 In practice, AFM nanoindentation has been successfully used for estimating Young's modulus, spring constant, breaking strength.4, 8 Fig. 6d illustrates AFM indentation process. Note that commercial AFM probes are generally sharp, and therefore a blunting procedure may be applied to avoid rupturing the nanosheet. The force spectroscopy typically features initial linear followed by nonlinear deformation (Fig. 6e). For the linear region, bending stiffness or spring constant can be obtained. At larger indentations, non-linear behavior is generally observed. The theory of a point load on a clamped thin film can predict its mechanical properties, which can be used to model experimental force curve to determine elastic moduli and ultimate strength. 27

In addition, an interesting recent study shows that grazing-incidence SAXS can identify 0.6 nm difference in average ligand-shell thickness between two sides of alky-ligated nanoparticle superlattice membranes.28 Hence, they called their membrane as Janus-like structures which were also proven by SERS measurement using a molecular tracer. Upon exposure to electron beam, the detached free-standing membranes can self-fold into tubular structures. Because the air-facing side has higher ligand density and less strain, the folding is always towards water-facing side which has lower ligand density and higher strain.

Applications. – *As soft surface enhanced Raman scattering (SERS) substrates*. The commercially available Klarite SERS substrate is based on evaporated gold on lithographically patterned silicon. It is rigid and opaque, preventing it from establishment of conformal contract with topologically complex real-world surfaces, such as banknotes and coins. Hence, it is impractical to use the Klarite substrate for direct identification of trace amount of chemicals. This limitation can be overcome by using soft plasmonic nanoparticle superlattice sheets (or plasmene nanosheets) which renders it possible to directly "attach and detect" (Fig.7a).14, 29 The elastic nature of nanosheets enables their conformal contact with topologically complex surfaces to position plasmonic field in close affinity with surface chemicals; their optical semitransparency enables direct spectral acquisition without the need of extracting trace amount of chemicals into solution; the uniform particle size/shape enables reliable spatial quantification.

Anticounterfeit. Nanosheet-constituent building blocks can carry optical signatures specific to nanoparticle size and shape;1 simultaneously, SERS molecular fingerprint vibrational information can be built into the nanosheets during synthesis.21 Thus, plasmonic nanoparticle superlattice sheets can serve as a dual-coded security label for banknotes (Fig. 7b). As a proof of concept, we have designed nine different plasmonic codes from gold nanospheres, gold rhombic dodecahedrals, and gold nanostars as building blocks. Each type of building blocks has three different sizes. In addition, we have chosen five additional SERS fingerprint barcodes. This means that we have generated 45 dually-coded security labels. Considering the choices of nanoparticle building blocks and SERS molecules, this approach can in principle offer virtually unlimited coding capacity.

Ionic gating. The interstices between nanoparticles in the nanosheets may be used for ionic gating applications. Usually, larger particle size leads to larger interparticle spacing. When nanosheets with two different nanoparticle sizes are assembled into a bilayer configuration, asymmetric cone-like ionic channels form.16 This geometrical asymmetry leads to diode-like I-V curves. Furthermore, a simulation map can be establish to describe the relationship between channel structures and ionic selectivity. By choosing different constituent particle size pairs, the current rectifying ratio can be tuned (Fig. 7c).

Stimuli-responsive. Ligand-based nanoparticle superlattice sheets can possess soft materials properties, such as stimuli-responsive properties. Fig. 7d shows that nearest neighbor

spacing in DNA-nanoparticle sheets is sensitive to ionic strength.18 Higher ionic strength screens charges so that DNA strands tend to collapse so that the interparticle spacing reduces. This has been proven by Synchrotron-based SAXS. In addition, plasmonic properties of ligand-based nanoparticle superlattice sheets may be sensitive to mechanical stimuli.22 When the lattice is stretched, interparticle spacing may increase, reducing plasmonic coupling, hence, causing spectral shift. This attribute may be used for strain gauge sensing applications.

Challenges and opportunities. – As is described above, the free-standing nanoparticle superlattice sheets are a special type of materials in the family of self-assemblies of nanocrystals. The mechanical flexibility endows this kind of 2D materials with novel properties and applications, which are difficult to achieve with substrate-supported and solution-state counterparts. Soft adhesive-like SERS substrate, 3D origami and ion-gating nanomembranes are representative examples.

Despite of encouraging progress made so far, scalable fabrication technologies to achieve defect-free structure remain the challenge. It is known that the nanoparticles are extremely difficult to manipulate due to complex nanoscale forces occurring at different temporal and spatial scales. To date, success is limited to only a few types of simple particle sizes and shapes; production of high-quality nanosheets at the macroscopic scales remain challenging. Soft capping ligands play crucial roles in regulating chemical potentials among nanoparticles in order to obtain 2D nanosheet assemblies. However, it remains illusive to control ligand-to-ligand interactions including steric hindrance, hydrogen bonding, electrostatic attraction/repulsion and bio-recognition forces at the desired temporal and spatial scales. Hence, it remains lack of a general design rule towards well-defined 2D nanosheet assemblies.

Free-standing nanoparticle superlattice sheets may be treated as nanoscale analogue of current 2D materials. However, they only arouse research interest from a few groups worldwide and only a few type of nanoparticle size/shapes were demonstrated. There are a diverse of other particle geometries, material and soft ligand composition, as well as hybrid binary or tertiary systems remain to be explored. While I acknowledge it is challenging task, modern experimental techniques such as SAXS, 3D structural tomography, optical microscopy in conjunction with multiscale modeling and simulation (molecular dynamics, coarse-grain model, Monte Carlo technique) may allow for establishment of useful design rules for the reliable fabrication of scalable nanoparticle superlattice sheets to complement and/or add new functions to current 2D materials family.

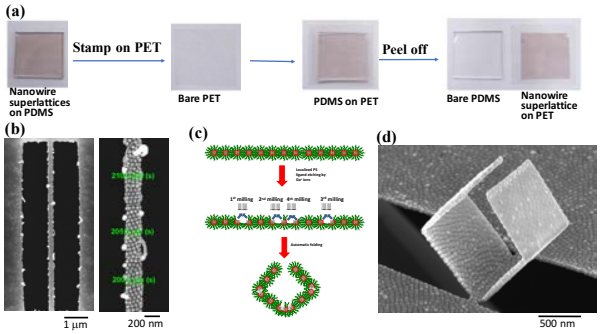

Fig. 1: Transferability and manufacturability of free-standing superlattices. (a) Transfer of nanowire superlattice membranes from PDMS to PET substrates; (b) Free-standing Au@Ag nanocube superlattice ribbons; (c) Schematic of fabrication of Au@Ag nanocube superlattice sheets into cube-like origami by focused-ion-beam lithography; (d) SEM image of cube-like origami from Au@Ag nanocube building blocks. Reproduced from reference 13, 9.

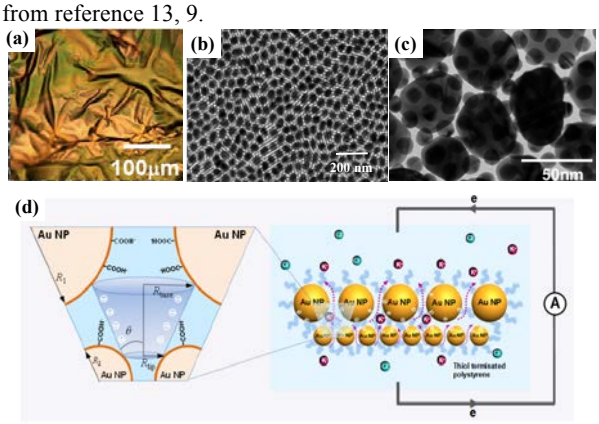

Fig. 2: Bilayered gold nanoparticle superlattice sheets as ionic transport membrane. (a) Optical image of bilayered nanoparticle superlattice membranes; (b-c) SEM images of bilayered nanoparticle superlattice membranes under two different magnifications; (d) Schematic of cone-like geometry enabling directional regulation of ionic transports. Reproduced from reference 16.

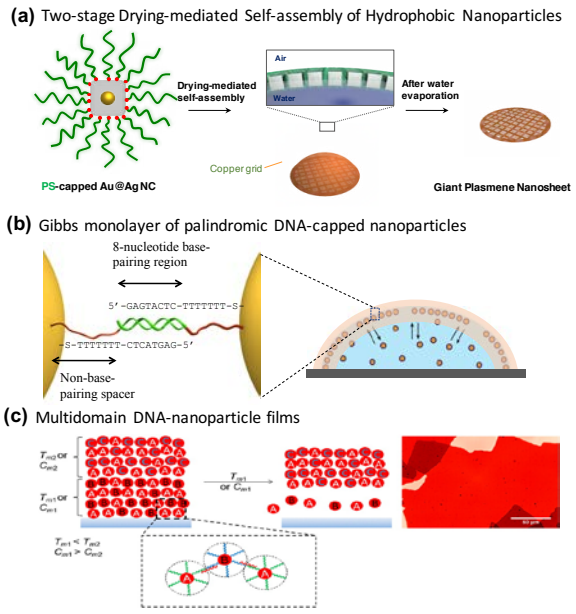

Fig. 3: Self-assembled nanosheets by entropy or enthalpy-driven processes. (a) Drying-mediated entropy-driven self-assembly of hydrophobic nanoparticles at the air/water interface; (b) Gibbs monolayered DNA-nanoparticle sheets by enthalpy-driven Watson-crick base-pairing forces; (c) DNA-based multidomain self-assembled gold nanoparticle films by enthalpy-driven Watson-crick base-pairing forces. Reproduced from reference 9, 18, 19.

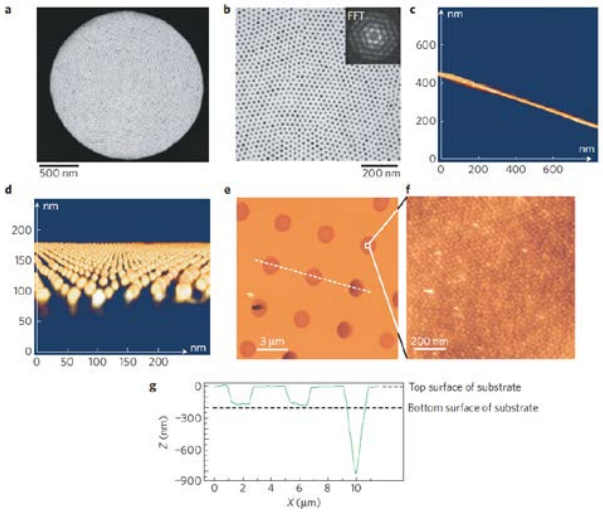

Fig. 4: Characterization of a free-standing, monolayered DNA-nanoparticle superlattice sheet. (a) TEM micrograph of a free-standing, monolayered DNA-nanoparticle superlattice sheet suspended over a 2-μm-diameter microhole in the silicon nitride substrate; (b) A higher-magnification TEM micrograph shows that nanoparticles are highly ordered yet well spaced. The inset shows a fast Fourier transform (FFT) of the image; (c,d) 3D Scanning TEM tomography reveals that the sheet is both monolayered and flat; (e) Characteristic AFM height image showing the presence of fully attached sheets and empty holes in the silicon nitride substrate; (f) High-resolution AFM image of the surface of a fully attached sheet showing highly ordered nanoparticles; (g) Cross-sectional height plot, corresponding to the dashed line in e, showing recessed sheets and an immeasurably deep hole in which no sheet formed. Reproduced from reference 8.

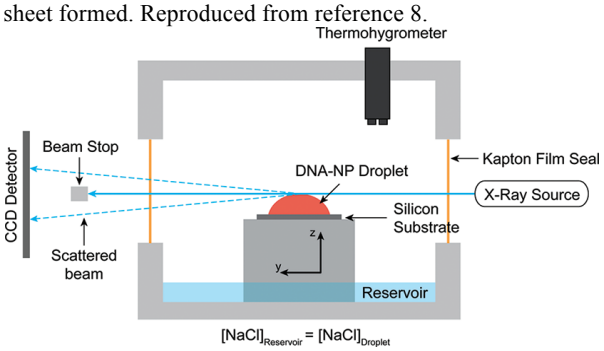

Fig. 5: Schematic of Synchrotron-based Small-Angle X-ray Scattering (SAXS) setup for probing spatial crystallization events of DNA-capped nanoparticles at the air/water interface. Reproduced from reference 18.

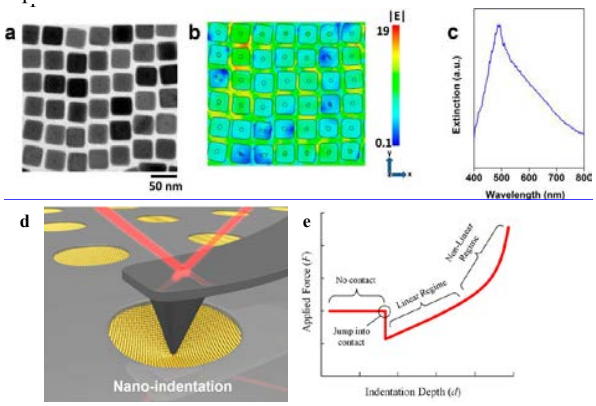

Fig. 6: Properties of free-standing nanoparticle superlattice sheets. (a) Representative TEM image for Au@Ag nanocube-based plasmene nanosheet; (b) Simulated near-field distributions when excited with light having a free space wavelength of 490 nm; (c) Experimental extinction spectrum of the Au@Ag nanocube-based plasmene sheet; (d) Nano-indentation with a nanoscale AFM probe; (e) A Typical AFM force–indentation curve showing consecutive events of no contact, jump in, linear and non-linear deformation of a free-standing nanoparticle superlattice sheet. Reproduced from reference 9, 26.

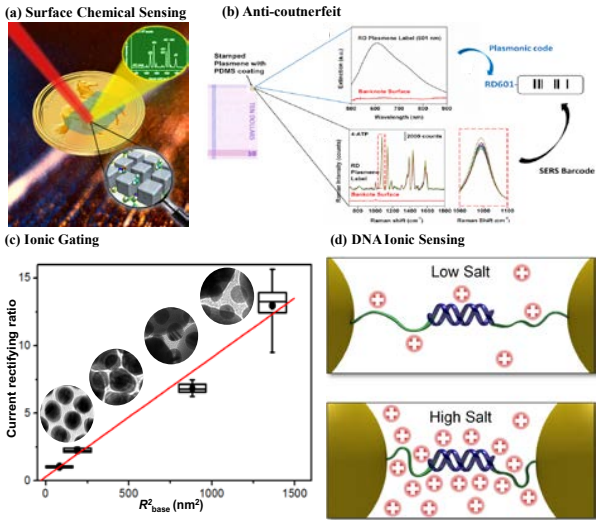

Fig. 7: Representative applications of free-standing nanoparticle superlattice sheets. (a) Application as soft, semitransparent SERS substrate for direct real-world surface chemical identifications; (b) Combination of plasmonic codes (sizes and shapes) with molecular codes (fingerprint vibrational signals) to offer dually-coded security labels for encryption applications; (c) asymmetric ionic regulation via bilayered nanoparticle superlattice sheets; (d) Palindramic DNA sequences are responsive to ionic strength. Reproduced from reference 29, 21, 16, 18.

***

I thank financial support from Australian Research Council via Discovery Grant scheme DP140100052, DP170102208. I also express great thanks to Ms Qianqian Shi for help edit the manuscript.

REFERENCES

1. Tan, S. J.; Campolongo, M. J.; Luo, D.; Cheng, W. L., Nature Nanotechnology 2011, 6 (5), 268-276.
2. Collier, C. P.; Saykally, R. J.; Shiang, J. J.; Henrichs, S. E.; Heath, J. R., Science 1997, 277 (5334), 1978-1981.
3. Courty, A.; Mermet, A.; Albouy, P. A.; Duval, E.; Pileni, M. P., Nature Materials 2005, 4 (5), 395-398.
4. Mueggenburg, K. E.; Lin, X. M.; Goldsmith, R. H.; Jaeger, H. M., Nature Materials 2007, 6 (9), 656-660.
5. Urban, J. J.; Talapin, D. V.; Shevchenko, E. V.; Kagan, C. R.; Murray, C. B., Nature Materials 2007, 6 (2), 115-121.
6. Pileni, M. P., Epl-Europhys Lett 2015, 109 (5).
7. Black, C. T.; Murray, C. B.; Sandstrom, R. L.; Sun, S. H., Science 2000, 290 (5494), 1131-1134.
8. Cheng, W. L.; Campolongo, M. J.; Cha, J. J.; Tan, S. J.; Umbach, C. C.; Muller, D. A.; Luo, D., Nat Mater 2009, 8 (6), 519-525.
9. Si, K. J.; Sikdar, D.; Chen, Y.; Eftekhari, F.; Xu, Z.; Tang, Y.; Xiong, W.; Guo, P.; Zhang, S.; Lu, Y.; Bao, Q.; Zhu, W.; Premaratne, M.; Cheng, W., ACS Nano 2014, 8 (11), 11086-11093.
10. Shi, Q.; Si, K. J.; Sikdar, D.; Yap, L. W.; Premaratne, M.; Cheng, W., ACS Nano 2016, 10 (1), 967-76.
11. Ng, K. C.; Udagedara, I. B.; Rukhlenko, I. D.; Chen, Y.; Tang, Y.; Premaratne, M.; Cheng, W., ACS Nano 2012, 6 (1), 925-934.
12. Auyeung, E.; Cutler, J. I.; Macfarlane, R. J.; Jones, M. R.; Wu, J. S.; Liu, G.; Zhang, K.; Osberg, K. D.; Mirkin, C. A., Nature Nanotechnology 2012, 7 (1), 24-28.
13. Chen, Y.; Zi, O.; Gu, M.; Cheng, W., Advanced Materials 2013, 25 (1), 80-85.
14. Chen, Y.; Si, K. J.; Sikdar, D.; Tang, Y.; Premaratne, M.; Cheng, W., Advanced Optical Materials 2015, 3 (7), 919-924.
15. Si, K. J.; Guo, P.; Shi, Q.; Cheng, W., Anal Chem 2015, 87 (10), 5263-5269.
16. Rao, S.; Si, K. J.; Yap, L. W.; Xiang, Y.; Cheng, W., ACS Nano 2015, 9 (11), 11218-24.
17. Si, K. J.; Chen, Y.; Cheng, W. L., Materials Today 2016, 19 (6), 363-364.
18. Campolongo, M. J.; Tan, S. J.; Smilgies, D. M.; Zhao, M.; Chen, Y.; Xhangolli, I.; Cheng, W. L.; Luo, D., ACS Nano 2011, 5 (10), 7978-7985.
19. Estephan, Z. G.; Qian, Z. X.; Lee, D.; Crocker, J. C.; Park, S. J., Nano Lett 2013, 13 (9), 4449-4455.
20. Shim, T. S.; Estephan, Z. G.; Qian, Z. X.; Prosser, J. H.; Lee, S. Y.; Chenoweth, D. M.; Lee, D.; Park, S. J.; Crocker, J. C., Nature Nanotechnology 2017, 12 (1), 41-47.
21. Si, K. J.; Sikdar, D.; Yap, L. W.; Foo, J. K. K.; Guo, P. Z.; Shi, Q. Q.; Premaratne, M.; Cheng, W. L., Advanced Optical Materials 2015, 3 (12), 1710-1717.
22. Guo, P.; Sikdar, D.; Huang, X.; Si, K. J.; Su, B.; Chen, Y.; Xiong, W.; Wei Yap, L.; Premaratne, M.; Cheng, W., J Phys Chem C 2014, 118 (46), 26816-26824.
23. Cheng, W. L.; Hartman, M. R.; Smilgies, D. M.; Long, R.; Campolongo, M. J.; Li, R. P.; Sekar, K.; Hui, C. Y.; Luo, D., Angewandte Chemie International Edition 2010, 49 (2), 380-384.
24. Park, S. Y.; Lytton-Jean, A. K. R.; Lee, B.; Weigand, S.; Schatz, G. C.; Mirkin, C. A., Nature 2008, 451 (7178), 553-556.
25. Kanjanaboos, P.; Lin, X. M.; Sader, J. E.; Rupich, S. M.; Jaeger, H. M.; Guest, J. R., Nano Lett 2013, 13 (5), 2158-2162.
26. Cheng, W.; Campolongo, M. J.; Tan, S. J.; Luo, D., Nano Today 2009, 4 (6), 482-493.
27. Wan, K. T.; Guo, S.; Dillard, D. A., Thin Solid Films 2003, 425 (1-2), 150-162.
28. Jiang, Z.; He, J. B.; Deshmukh, S. A.; Kanjanaboos, P.; Kamath, G.; Wang, Y. F.; Sankaranarayanan, S. K. R. S.; Wang, J.; Jaeger,

H. M.; Lin, X. M., Nature Materials 2015, 14 (9), 912.
29. Chen, Y.; Si, K. J.; Sikdar, D.; Tang, Y.; Premaratne, M.; Cheng, W., Advanced Optical Materials 2015, 3 (7), 918-918.